

Relationship Between Space-Vector Modulation and Three-Phase Carrier-Based PWM: A Comprehensive Analysis

Keliang Zhou and Danwei Wang, *Member, IEEE*

Abstract—This paper comprehensively analyzes the relationship between space-vector modulation and three-phase carrier-based pulsedwidth modulation (PWM). The relationships involved, such as the relationship between modulation signals (including zero-sequence component and fundamental components) and space vectors, the relationship between the modulation signals and the space-vector sectors, the relationship between the switching pattern of space-vector modulation and the type of carrier, and the relationship between the distribution of zero vectors and different zero-sequence signal are systematically established. All the relationships provide a bidirectional bridge for the transformation between carrier-based PWM modulators and space-vector modulation modulators. It is shown that all the drawn conclusions are independent of the load type. Furthermore, the implementations of both space-vector modulation and carrier-based PWM in a closed-loop feedback converter are discussed.

Index Terms—Carrier-based pulsedwidth modulation, space-vector pulsedwidth modulation.

I. INTRODUCTION

PULSEWIDTH modulation (PWM) has been studied extensively during the past decades. Many different PWM methods have been developed to achieve the following aims: wide linear modulation range; less switching loss; less total harmonic distortion (THD) in the spectrum of switching waveform; and easy implementation and less computation time.

For a long period, carrier-based PWM methods [1] were widely used in most applications. The earliest modulation signals for carrier-based PWM are sinusoidal. The use of an injected zero-sequence signal for a three-phase inverter [2] initiated the research on nonsinusoidal carrier-based PWM [3]–[7]. Different zero-sequence signals lead to different nonsinusoidal PWM modulators. Compared with sinusoidal three-phase PWM, nonsinusoidal three-phase PWM can extend the linear modulation range for line-to-line voltages.

With the development of microprocessors, space-vector modulation has become one of the most important PWM methods for three-phase converters [8]–[15]. It uses the space-vector concept to compute the duty cycle of the switches. It is simply the digital implementation of PWM modulators. An aptitude for

easy digital implementation and wide linear modulation range for output line-to-line voltages are the notable features of space vector modulation.

The comprehensive relation of the two PWM methods provides a platform not only to transform from one to another, but also to develop different performance PWM modulators. Therefore, many attempts have been made to unite the two types of PWM methods [16], [17]. The relationship between space vectors and fundamental modulation signals was derived in [18]–[21]. Reference [17] suggested the relationship between common-node voltage (*zero-sequence voltage*) and the space vectors on the basis of a three-phase inverter with a symmetrical Y-connected load. However, the dependence on the load [17] hinders the universal significance of its drawn conclusions.

This paper aims to reveal the comprehensive relationship between space-vector modulation and carrier-based PWM. The relationship between modulation signals and voltage vectors, the relationship between zero-sequence signal and space vectors, the relationship between the modulation signals and the vector sectors, the relationship between the sequence of space vectors and the type of carrier, and the relationship between the distribution of zero vectors and different carrier-based PWM modulators are systematically investigated without dependence on the load type. Furthermore, the implementations of these two PWM methods in the feedback closed-loop converter are discussed with corresponding solutions. Simulation results are provided to validate the drawn conclusions.

II. CARRIER-BASED PWM

A. Basic Properties

A carrier-based PWM modulator is comprised of modulation signals and carrier signal.

The operation of PWM can be divided into two modes [22], [23].

- 1) *Linear Mode*.—In the linear mode, the peak of a modulation signal is less than or equal to the peak of the carrier signal. When the carrier frequency f_{car} is greater than $20\times$ modulation signal frequency f , the gain of PWM $G \approx 1$.
- 2) *Nonlinear Mode*.—When the peak of a modulation signal is greater than the peak of the carrier signal, overmodulation occurs with $G < 1$. The six-step mode marks the end of the nonlinear mode. The THD of output switched waveforms increases.

Manuscript received November 3, 1999; revised July 6, 2001. Abstract published on the Internet December 5, 2001.

The authors are with the School of Electrical and Electronic Engineering Nanyang Technological University, Singapore 639798 (e-mail:edwwang@ntu.edu.sg).

Publisher Item Identifier S 0278-0046(02)00933-4.

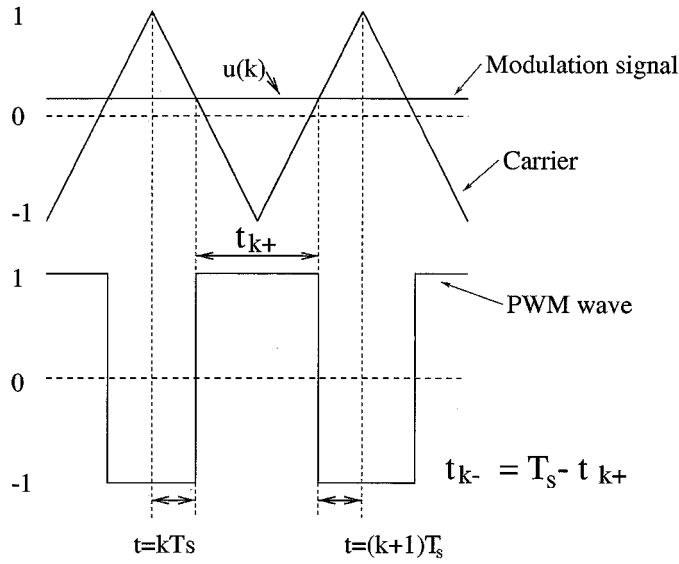


Fig. 1. Two-level carrier-based PWM.

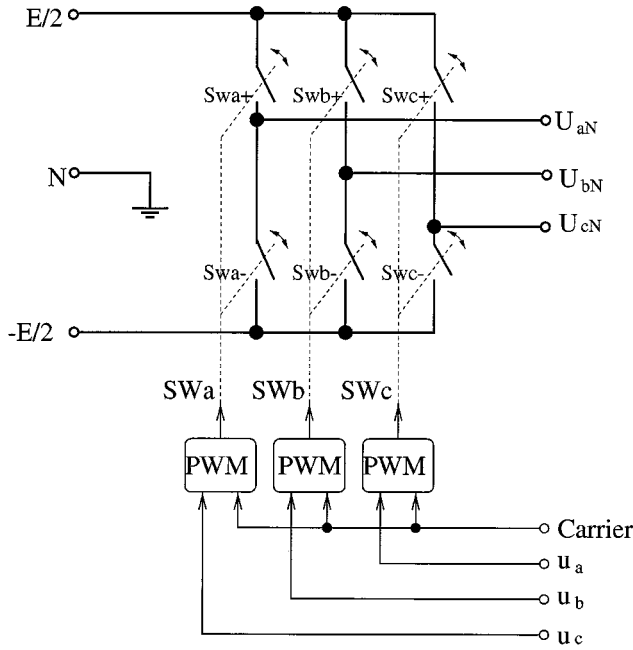


Fig. 2. Three-phase PWM inverter.

As shown in Fig. 1, in the linear mode, for carrier-based two-level PWM modulators, we have

$$\begin{aligned} t_{k+} - t_{k-} &= u_k T_s \\ t_{k+} &= \frac{1}{2}(1 + u_k) T_s \\ t_{k-} &= \frac{1}{2}(1 - u_k) T_s \end{aligned} \quad (1)$$

where t_{k+} and t_{k-} are the positive and the negative pulsewidths in the k th sampling interval, respectively; $u(k)$ is the normalized amplitude of modulation signal in the k th sampling interval ($|u(k)| \leq 1$); and the normalized peak value of the carrier signal is 1. Equation (1) is usually referred to as the *Equal Voltage—Second principle* [14], [18], [24].

Fig. 2 shows a three-phase PWM inverter without consideration of the load type. In the linear modulation range, ne-

glecting high-order harmonics, the output line-to-neutral voltages U_{iN} ($i = a, b, c$) satisfy

$$U_{iN} = \frac{E}{2} u_i \quad (i = a, b, c) \quad (2)$$

where N is the neutral point of the dc bus.

When overmodulation occurs, i.e., $|u(k)| > 1$, (1) and (2) are not satisfied.

B. Carrier-Based PWM

A universal representation of modulation signals $u_i(t)$ ($i = a, b, c$) for three-phase carrier PWM modulators is as follows:

$$u_i(t) = u_i^*(t) + e_i(t) \quad (3)$$

where $e_i(t)$ are injected harmonics, and u_i^* are called fundamental signals that are three-phase symmetrical sinusoidal signals as follows:

$$\begin{aligned} u_a^*(t) &= m \sin \omega t \\ u_b^*(t) &= m \sin \left(\omega t + \frac{2\pi}{3} \right) \\ u_c^*(t) &= m \sin \left(\omega t + \frac{4\pi}{3} \right) \end{aligned} \quad (4)$$

where m is the modulation index, and $u_a^*(t) + u_b^*(t) + u_c^*(t) = 0$.

According to (2) and (4), the output line-to-neutral voltages U_{iN} ($i = a, b, c$) (as shown in Fig. 2) are

$$\begin{aligned} U_{aN}(t) &= \frac{E}{2} [m \sin \omega t + e_i(t)] \\ U_{bN}(t) &= \frac{E}{2} [m \sin(\omega t + \frac{2\pi}{3}) + e_i(t)] \\ U_{cN}(t) &= \frac{E}{2} [m \sin(\omega t + \frac{4\pi}{3}) + e_i(t)]. \end{aligned} \quad (5)$$

The output line-to-line voltages U_{ab} , U_{bc} , and U_{ca} are

$$\begin{aligned} U_{ab}(t) &= U_{aN}(t) - U_{bN}(t) \\ &= \frac{E}{2} \sqrt{3} m \sin \left(\omega t + \frac{\pi}{6} \right) \\ U_{bc}(t) &= \frac{E}{2} \sqrt{3} m \sin \left(\omega t + \frac{5\pi}{6} \right) \\ U_{ca}(t) &= \frac{E}{2} \sqrt{3} m \sin \left(\omega t + \frac{3\pi}{2} \right). \end{aligned} \quad (6)$$

In the linear modulation range, (5), (6), and $|u_i| \leq 1$ show that output line-to-line voltages are equal to or less than dc-bus voltage E . Therefore, the possible maximum modulation index m_{\max} is $2/\sqrt{3}$ in the linear range, and we have

$$-1 - u_{\min}^*(t) \leq e_i(t) \leq 1 - u_{\max}^*(t) \quad (7)$$

where $u_{\min}^*(t) = \min(u_a^*(t), u_b^*(t), u_c^*(t))$, and $u_{\max}^*(t) = \max(u_a^*(t), u_b^*(t), u_c^*(t))$.

It is clear that the injected harmonics $e_i(t)$ do not appear in the line-to-line voltages. Therefore, $e_i(t)$ is usually called as *zero sequence signal* [14], [21], and $e_i(t)$ can be calculated by

$$e_i(t) = \frac{1}{3}(u_a(t) + u_b(t) + u_c(t)). \quad (8)$$

$e_i(t) = 0$ yields *sinusoidal PWM*. In the linear range, from (4) and (5) and $|u_i| \leq 1$, we have $m_{\max} = 1$ and the maximum

output line-to-line voltages are $\sqrt{3}/2E$. When $m > 1$, over-modulation occurs.

When $e_i(t) \neq 0$, *nonsinusoidal* PWM occurs. When $e_i(t)$ is a suitable signal, such as $e_i(t) = m/6 \sin(\omega t)$ [2], all the tops of $u_i^*(t)$ are cut by $e_i(t)$. m_{\max} is $2/\sqrt{3}$ and the maximum output line-to-line voltages reach E in the linear range. Different $e_i(t)$ leads to different carrier-based PWM modulators for three-phase converters [4], [5]. It shows that suitable $e_i(t)$ can extend the linear modulation range of three-phase RSPWM modulators.

In terms of the switching characteristics, PWM schemes can be divided into continuous PWM and discontinuous PWM in the linear modulation range.

For continuous PWM schemes, $-1 - u_{\min}^*(t) < e_i(t) < 1 - u_{\max}^*(t)$ ($m \leq 2/\sqrt{3}$). Therefore, in each carrier signal period, each output of the converter legs is switching between the positive or negative rail of the dc link, whereas, for discontinuous PWM schemes, in the linear modulation range, the zero-sequence component $e_i(t) = -1 - u_{\min}^*(t)$ or $e_i(t) = 1 - u_{\max}^*(t)$. Obviously, in each carrier cycle, one modulation signal will be equal to ± 1 and the corresponding leg is tied to the positive or negative rail of the dc link without switching actions. Thus, from an average view, compared with continuous PWM schemes, discontinuous PWM schemes can reduce the average switching frequency by 33% and cause less switching loss.

III. SPACE-VECTOR PWM

For the three-phase two-level PWM inverter as shown in Fig. 2, the switch function is defined by (9), shown at the bottom of the page. where $i = a, b, c$; "1" denotes $E/2$ at the inverter output (a, b, c) with reference to point N ; "0" denotes $-E/2$; N is the neutral point of the dc bus.

There are eight switch states $\vec{S}_i = (SW_a SW_b SW_c)$, $i = 0, 1, \dots, 7$ (as shown in Fig. 3). The output voltages of the inverter are composed by these eight switch states. Define eight voltage vectors $\vec{U}_0 = [000], \dots, \vec{U}_7 = [111]$ corresponding to the switch states $\vec{S}_0, \dots, \vec{S}_7$, respectively. The lengths of vectors $\vec{U}_1, \dots, \vec{U}_6$ are unity and the lengths of \vec{U}_0 and \vec{U}_7 are zero, and these eight vectors form the voltage-vector space as displayed in Fig. 3. The voltage-vector space is divided up into six sectors.

In the vector space, according to the equivalence principle, the following operation rules are obeyed:

$$\begin{aligned} \vec{U}_1 &= -\vec{U}_4 \\ \vec{U}_2 &= -\vec{U}_5 \\ \vec{U}_3 &= -\vec{U}_6 \\ \vec{U}_0 &= \vec{U}_7 = \vec{0} \\ \vec{U}_1 + \vec{U}_3 + \vec{U}_5 &= \vec{0}. \end{aligned} \quad (10)$$

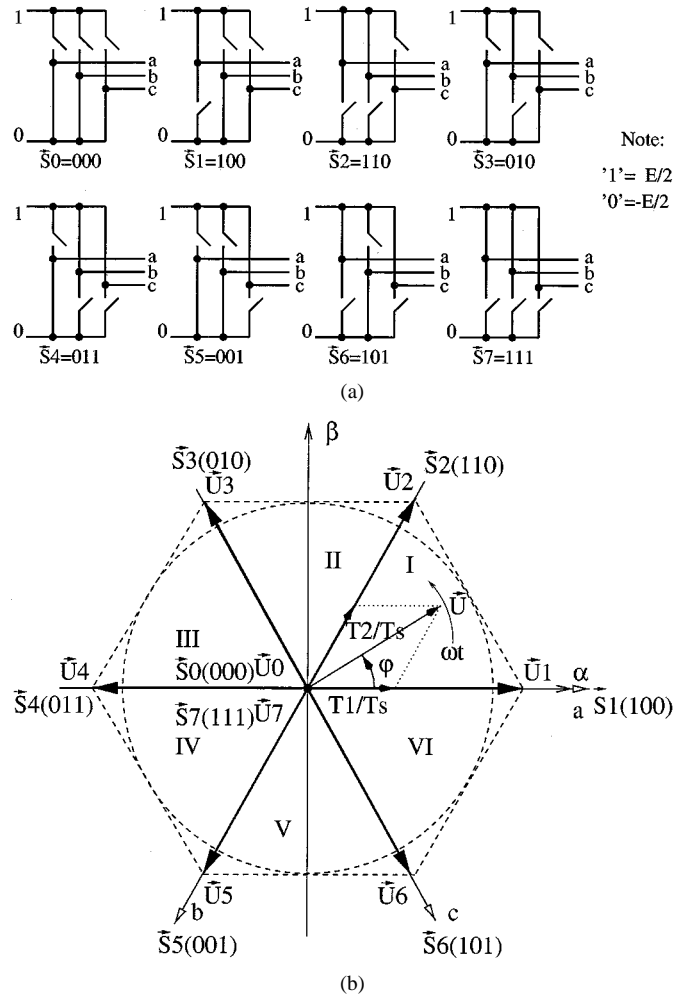


Fig. 3. Space vectors. (a) Eight switching states. (b) Voltage vector space.

In one sampling interval, the output voltage vector \vec{U} can be written as

$$\vec{U}(t) = \frac{t_0}{T_s} \vec{U}_0 + \frac{t_1}{T_s} \vec{U}_1 + \dots + \frac{t_7}{T_s} \vec{U}_7 \quad (11)$$

where t_0, t_1, \dots, t_7 are the turn-on time of the vectors $\vec{U}_1, \dots, \vec{U}_7$; $t_0, t_1, \dots, t_7 \geq 0$, $\sum_{i=0}^7 t_i = T_s$; and T_s is the sampling time.

According to (10) and (11), the decomposition of \vec{U} into $\vec{U}_1, \vec{U}_2, \dots, \vec{U}_7$ has infinite ways. However, in order to reduce the number of switching actions and make full use of active turn-on time for space vectors, the vector \vec{U} is commonly split into the two nearest adjacent voltage vectors and zero vectors \vec{U}_0 and \vec{U}_7 in an arbitrary sector. For example, in sector I, in one sampling interval, vector \vec{U} can be expressed as

$$\vec{U} = \frac{T_1}{T_s} \vec{U}_1 + \frac{T_2}{T_s} \vec{U}_2 + \frac{T_7}{T_s} \vec{U}_7 + \frac{T_0}{T_s} \vec{U}_0 \quad (12)$$

where $T_s - T_1 - T_2 = T_0 + T_7 \geq 0$, $T_0 \geq 0$ and $T_7 \geq 0$.

$$SW_i = \begin{cases} 1, & \text{the upper switch } SW_{i+} \text{ is on and the bottom switch } SW_{i-} \text{ is off} \\ 0, & \text{the upper switch } SW_{i+} \text{ is off and the bottom switch } SW_{i-} \text{ is on} \end{cases} \quad (9)$$

TABLE I
 SPACE-VECTOR-MODULATION ALGORITHM

Sector I ($0 \leq \omega t \leq \frac{\pi}{3}$)	Sector II ($\frac{\pi}{3} \leq \omega t \leq \frac{2\pi}{3}$)	Sector III ($\frac{2\pi}{3} \leq \omega t \leq \pi$)
$T_1 = \frac{\sqrt{3}}{2}mT_s \cos(\omega t + \frac{\pi}{6})$	$T_2 = \frac{\sqrt{3}}{2}mT_s \cos(\omega t + \frac{11\pi}{6})$	$T_3 = \frac{\sqrt{3}}{2}mT_s \cos(\omega t + \frac{3\pi}{2})$
$T_2 = \frac{\sqrt{3}}{2}mT_s \cos(\omega t + \frac{3\pi}{2})$	$T_3 = \frac{\sqrt{3}}{2}mT_s \cos(\omega t + \frac{7\pi}{6})$	$T_4 = \frac{\sqrt{3}}{2}mT_s \cos(\omega t + \frac{5\pi}{6})$
$T_0 + T_7 = T_s - T_1 - T_2$	$T_0 + T_7 = T_s - T_2 - T_3$	$T_0 + T_7 = T_s - T_3 - T_4$
Sector IV ($\pi \leq \omega t \leq \frac{4\pi}{3}$)	Sector V ($\frac{4\pi}{3} \leq \omega t \leq \frac{5\pi}{3}$)	Sector VI ($\frac{5\pi}{3} \leq \omega t \leq 2\pi$)
$T_4 = \frac{\sqrt{3}}{2}mT_s \cos(\omega t + \frac{7\pi}{6})$	$T_5 = \frac{\sqrt{3}}{2}mT_s \cos(\omega t + \frac{5\pi}{6})$	$T_6 = \frac{\sqrt{3}}{2}mT_s \cos(\omega t + \frac{\pi}{2})$
$T_5 = \frac{\sqrt{3}}{2}mT_s \cos(\omega t + \frac{\pi}{2})$	$T_6 = \frac{\sqrt{3}}{2}mT_s \cos(\omega t + \frac{\pi}{6})$	$T_1 = \frac{\sqrt{3}}{2}mT_s \cos(\omega t + \frac{11\pi}{6})$
$T_0 + T_7 = T_s - T_4 - T_5$	$T_0 + T_7 = T_s - T_5 - T_6$	$T_0 + T_7 = T_s - T_1 - T_6$

Let the length of \vec{U} be m^*E , then we have

$$\frac{m^*}{\sin \frac{2\pi}{3}} = \frac{T_1}{T_s} \frac{1}{\sin(\frac{\pi}{3} - \varphi)} = \frac{T_2}{T_s} \frac{1}{\sin \varphi}. \quad (13)$$

Thus,

$$\begin{aligned} \frac{T_1}{T_s} &= \frac{2}{\sqrt{3}}m^* \sin(\frac{\pi}{3} - \omega t) = \frac{2}{\sqrt{3}}m^* \cos(\omega t + \frac{\pi}{6}) \\ \frac{T_2}{T_s} &= \frac{2}{\sqrt{3}}m^* \sin \omega t = \frac{2}{\sqrt{3}}m^* \cos(\omega t + \frac{3\pi}{2}) \\ T_0 + T_7 &= T_s - T_1 - T_2 \end{aligned} \quad (14)$$

where $2n\pi \leq \omega t = \varphi \leq 2n\pi + \pi/3$.

The length and angle of \vec{U} are determined by vectors $\vec{U}_1, \vec{U}_2, \dots, \vec{U}_6$ that are called *active vectors*, and \vec{U}_0, \vec{U}_7 are called *zero vectors*. Decomposition of \vec{U} in all six sectors is shown in Table I. Equations (12) and (13) are the commonly used formulation of the space-vector modulation modulator. It is shown that the turn-on times $T_i (i = 1, \dots, 6)$ for *active vectors* are identical in a different space PWM modulator. The different distribution of T_0 and T_7 for *zero vectors* yields different space-vector PWM modulators.

There are not separate modulation signals in each of the three phases in space-vector modulation technique [3]. Instead, a voltage vector is processed as a whole [8]. For space-vector modulation, the boundary between the linear modulation range and the overmodulation range in vector sector I is

$$\begin{aligned} T_s &= T_1 + T_2 \\ T_7 &= T_0 = 0. \end{aligned} \quad (15)$$

From (14) and (15), we have

$$\frac{m^*}{1} = \frac{\sin \frac{\pi}{3}}{\sin(\frac{2\pi}{3} - \varphi)}. \quad (16)$$

Therefore, the boundary between the linear modulation range and the overmodulation range is the hexagon [3], [15] in Fig. 4. The linear modulation range is located within the hexagon. If the voltage vector \vec{U} exceeds the hexagon, as calculated from (14), $T_1 + T_2$ becomes greater than T_s and unrealizable. Thus, the overmodulation region for space-vector modulation is outside the hexagon. In the six-step mode, the switching sequence

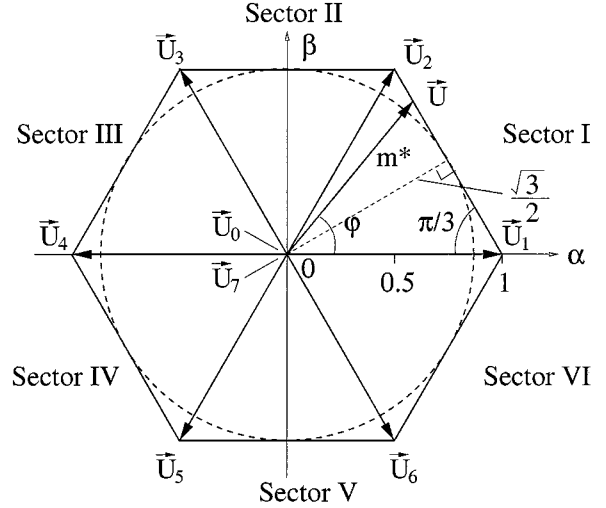


Fig. 4. Modulation range for space-vector modulation.

is $\vec{S}_1 - \vec{S}_2 - \vec{S}_3 - \vec{S}_4 - \vec{S}_5 - \vec{S}_6 - \vec{S}_1 \dots$ [3]. Furthermore, it should be pointed out that the trajectory of voltage vector \vec{U} should be circular while maintaining sinusoidal output line-to-line voltages. From Fig. 4 and (20), in the linear modulation range, when the length m^*E of $\vec{U} = \sqrt{3}/2E$, the trajectory of \vec{U} becomes the inscribed circle of the hexagon and the maximum amplitude of sinusoidal line-to-line voltages is the dc-bus voltage E . [12], [15], providing several useful overmodulation strategies for space-vector modulation.

Moreover, for space-vector PWM, there is a degree of freedom in the choice of zero vectors in one switching cycle, i.e., whether \vec{U}_0 or \vec{U}_7 or both.

For continuous space-vector schemes, in the linear modulation range, both \vec{U}_0 and \vec{U}_7 are used in one switching cycle, that is, $T_7 > 0$ and $T_0 > 0$.

For discontinuous space-vector schemes, in the linear modulation range, only \vec{U}_0 or only \vec{U}_7 is used in one switching cycle, that is, $T_7 = 0$ or $T_0 = 0$.

IV. RELATIONSHIP BETWEEN CARRIER-BASED PWM AND SPACE-VECTOR PWM

A. Modulation Signals and Space Vectors

Comparison between the two-level carrier-based PWM and the space-vector modulation in sector I [18] is illustrated in

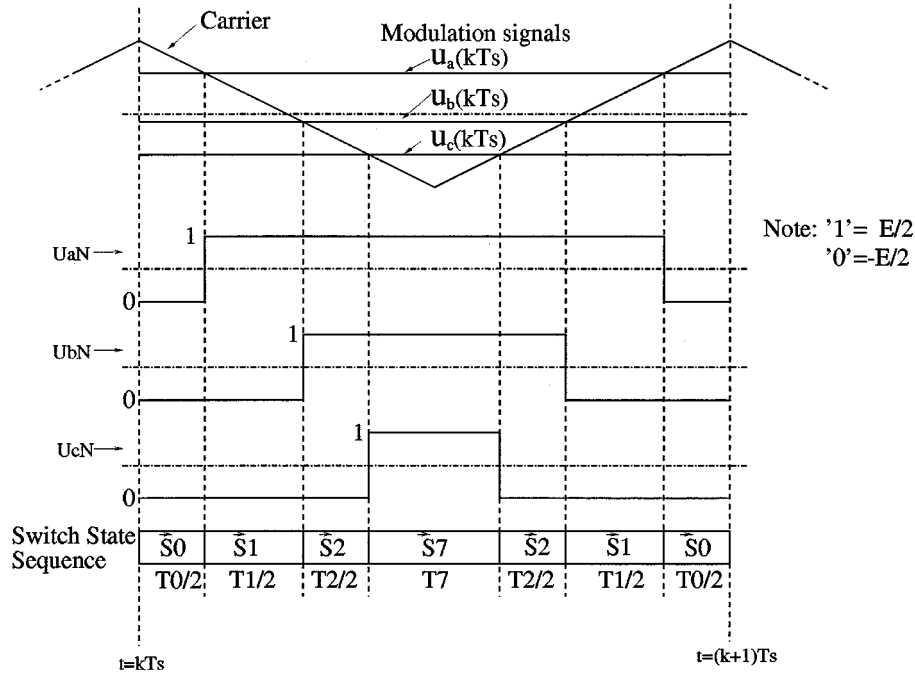


Fig. 5. Carrier-based PWM and space-vector modulation in sector I.

TABLE II
ZERO-SEQUENCE $e_i(t)$ AND SPACE VECTORS

Sector NO.	Space Voltage Vectors	Zero Sequence $e_i(t)$
I	$T_s = T_1 + T_2 + T_0 + T_7$	$e_i(t) = (-\frac{T_0}{T_s} - \frac{1}{3}\frac{T_1}{T_s} + \frac{1}{3}\frac{T_2}{T_s} + \frac{T_7}{T_s})$
II	$T_s = T_2 + T_3 + T_0 + T_7$	$e_i(t) = (-\frac{T_0}{T_s} + \frac{1}{3}\frac{T_2}{T_s} - \frac{1}{3}\frac{T_3}{T_s} + \frac{T_7}{T_s})$
III	$T_s = T_3 + T_4 + T_0 + T_7$	$e_i(t) = (-\frac{T_0}{T_s} - \frac{1}{3}\frac{T_3}{T_s} + \frac{1}{3}\frac{T_4}{T_s} + \frac{T_7}{T_s})$
IV	$T_s = T_4 + T_5 + T_0 + T_7$	$e_i(t) = (-\frac{T_0}{T_s} + \frac{1}{3}\frac{T_4}{T_s} - \frac{1}{3}\frac{T_5}{T_s} + \frac{T_7}{T_s})$
V	$T_s = T_5 + T_6 + T_0 + T_7$	$e_i(t) = (-\frac{T_0}{T_s} - \frac{1}{3}\frac{T_5}{T_s} + \frac{1}{3}\frac{T_6}{T_s} + \frac{T_7}{T_s})$
VI	$T_s = T_6 + T_1 + T_0 + T_7$	$e_i(t) = (-\frac{T_0}{T_s} + \frac{1}{3}\frac{T_6}{T_s} - \frac{1}{3}\frac{T_1}{T_s} + \frac{T_7}{T_s})$

Fig. 5. Based on the *Equal Voltage-Second* principle and Fig. 5, we have

$$\begin{aligned}
 U_{aN}T_s &= \frac{E}{2}(u_a^* + e_i)T_s = \frac{E}{2}(T_1 + T_2 + T_7 - T_0) \\
 U_{bN}T_s &= \frac{E}{2}(u_b^* + e_i)T_s = \frac{E}{2}(T_2 + T_7 - T_0 - T_1) \\
 U_{cN}T_s &= \frac{E}{2}(u_c^* + e_i)T_s = \frac{E}{2}(-T_1 - T_2 + T_7 - T_0).
 \end{aligned} \quad (17)$$

Thus,

$$\begin{aligned}
 u_a &= \frac{(T_1 + T_2 + T_7 - T_0)}{T_s} \\
 u_b &= \frac{(T_2 + T_7 - T_0 - T_1)}{T_s} \\
 u_c &= \frac{(-T_1 - T_2 + T_7 - T_0)}{T_s}.
 \end{aligned} \quad (18)$$

From (8) and (18), the zero-sequence signal $e_i(t)$ is calculated by

$$e_i = \frac{1}{3}(u_a + u_b + u_c) = -\frac{T_0}{T_s} - \frac{1}{3}\frac{T_1}{T_s} + \frac{1}{3}\frac{T_2}{T_s} + \frac{T_7}{T_s}.$$

$$(19) \quad T_0 + T_7 = T_s - T_1 - T_2.$$

The representations of $e_i(t)$ in the other five sectors are listed in Table II.

Equations (18) and (19) represent the relationship between the modulation signals and the space vectors. Therefore, an arbitrary carrier-based PWM modulator can be easily transformed into an equivalent space-vector modulation modulator. It seems that (19) is the same as the formulation for common-node voltage in [17]. However, a symmetrical Y-connected load with a common node is connected with the inverter in [17]. Equation (19) is independent of this assumption. Equations (18) and (19) are of universal significance.

B. Transformations Between Modulation Signals and Space Vectors

According to (6) and (17), we have

$$U_{ab}T_s = (U_{aN} - U_{bN})T_s = \frac{E}{2}(u_a^* - u_b^*)T_s = ET_1$$

$$U_{bc}T_s = (U_{bN} - U_{cN})T_s = \frac{E}{2}(u_b^* - u_c^*)T_s = ET_2$$

$$U_{ca}T_s = (U_{cN} - U_{aN})T_s = \frac{E}{2}(u_c^* - u_a^*)T_s = -E(T_1 + T_2)$$

$$(20)$$

TABLE III
 FUNDAMENTAL SIGNALS AND SPACE VECTORS

Sector I	Sector II	Sector III
$u_a^* - u_b^* = \frac{2T_1}{T_s}$	$u_a^* - u_b^* = -\frac{2T_1}{T_s}$	$u_b^* - u_c^* = \frac{2T_1}{T_s}$
$u_b^* - u_c^* = \frac{2T_2}{T_s}$	$u_c^* - u_a^* = -\frac{2T_2}{T_s}$	$u_c^* - u_a^* = \frac{2T_2}{T_s}$
Sector IV	Sector V	Sector VI
$u_a^* - u_b^* = -\frac{2T_1}{T_s}$	$u_a^* - u_b^* = \frac{2T_1}{T_s}$	$u_b^* - u_c^* = -\frac{2T_1}{T_s}$
$u_b^* - u_c^* = -\frac{2T_2}{T_s}$	$u_c^* - u_a^* = \frac{2T_2}{T_s}$	$u_c^* - u_a^* = -\frac{2T_2}{T_s}$

Thus,

$$\begin{aligned} u_a^* - u_b^* &= \frac{2T_1}{T_s} \\ u_b^* - u_c^* &= \frac{2T_2}{T_s}. \end{aligned} \quad (21)$$

Equation (20) shows the direct relationship between the line-to-line voltages and the space vectors in sector I. It also indicates that the output line-to-line voltages are determined by the *active vectors*, not the *zero vectors*. Equation (21) shows the relationship between the fundamental signals and the space vectors in sector I. The relationships between the fundamental signals and the space vectors in all six sectors are listed in Table III.

From Table I, T_1 and T_2 are calculated as follows:

$$\begin{aligned} \frac{T_1}{T_s} &= \frac{\sqrt{3}}{2} m \sin\left(\frac{\pi}{3} - \omega t\right) \\ \frac{T_2}{T_s} &= \frac{\sqrt{3}}{2} m \sin \omega t \\ T_0 + T_7 &= T_s - T_1 - T_2 \end{aligned} \quad (22)$$

where $\varphi = \omega t$ is defined as shown in Fig. 3

Comparing (14) with (22) leads to the relationship between length coefficient m^* of \vec{U} and modulation index m of the three-phase carrier-based PWM as follows

$$m^* = \frac{3}{4} m. \quad (23)$$

As shown in Fig. 3, we have

$$\begin{aligned} \tan(\varphi) &= \frac{T_\beta}{T_\alpha} \\ \frac{T_\alpha}{T_s} &= m^* \cos \varphi \\ \frac{T_\beta}{T_s} &= m^* \sin \varphi. \end{aligned} \quad (24)$$

Thus, T_1 and T_2 can be expressed as

$$\begin{aligned} \frac{T_1}{T_s} &= \frac{\sqrt{3}}{2} m \sin\left(\frac{\pi}{3} - \omega t\right) = \frac{T_\alpha}{T_s} - \frac{1}{\sqrt{3}} \frac{T_\beta}{T_s} \\ \frac{T_2}{T_s} &= \frac{\sqrt{3}}{2} m \sin(\omega t) = \frac{2}{\sqrt{3}} \frac{T_\beta}{T_s}. \end{aligned} \quad (25)$$

Therefore, according to (21) and (25), bidirectional transformations between fundamental signals in the (a, b, c) plane and active space vectors in the (α, β) plane are derived as follows:

$$\begin{pmatrix} \frac{T_\alpha}{T_s} \\ \frac{T_\beta}{T_s} \end{pmatrix} = \frac{1}{2} \begin{pmatrix} 1 & -\frac{1}{2} & -\frac{1}{2} \\ 0 & \frac{\sqrt{3}}{2} & -\frac{\sqrt{3}}{2} \end{pmatrix} \begin{pmatrix} u_a^* \\ u_b^* \\ u_c^* \end{pmatrix} \quad (26)$$

and

$$\begin{pmatrix} u_a^* \\ u_b^* \\ u_c^* \end{pmatrix} = \frac{4}{3} \begin{pmatrix} 1 & 0 \\ -\frac{1}{2} & \frac{\sqrt{3}}{2} \\ -\frac{1}{2} & -\frac{\sqrt{3}}{2} \end{pmatrix} \begin{pmatrix} \frac{T_\alpha}{T_s} \\ \frac{T_\beta}{T_s} \end{pmatrix}. \quad (27)$$

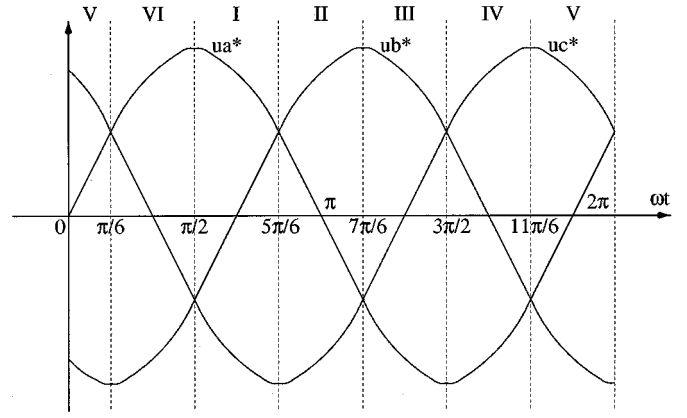


Fig. 6. Relationship between vector sector and fundamental modulation signals.

Equations (26) and (27) are the well-known 3/2 transformation and 2/3 transformation, respectively. Because of the symmetry of space sectors, the above transformations can be extended to all other five sectors.

C. Modulation Signals and Space-Vector Sectors

The relationships between the modulation signals and the space-vector sectors are displayed in Fig. 6 and Table IV.

D. Distribution of Zero Vectors and Zero-Sequence Signal

For space-vector modulation, due to $T_0 + T_7 = T_s - T_1 - T_2$, there are infinite different ways to distribute T_0 and T_7 . Different distributions of T_0 and T_7 yield different space-vector modulation modulators. A unified representation for the distribution of T_0 and T_7 in sector I can be written as

$$\begin{aligned} T_7 &= K_0(\omega t) T_{\text{zero}} \\ T_0 &= (1 - K_0(\omega t)) T_{\text{zero}} \\ T_{\text{zero}} &= T_s - T_1 - T_2 \end{aligned} \quad (28)$$

where $1 \geq K_0(\omega t) \geq 0$; $T_0 \geq 0$, $T_7 \geq 0$; T_1 and T_2 are determined by (22). When $1 \geq K_0(\omega t) = k_0 = \text{const} \geq 0$, the corresponding space-vector PWM modulators have been discussed in [18], whereas, a carrier-based PWM modulator is determined by its unique zero-sequence signal and a unified representation for $c_i(t)$

$$\begin{aligned} c_i &= K_0(\omega t)(1 - u_{\text{max}}^*) + (1 - K_0(\omega t))(-1 - u_{\text{min}}^*) \\ &= k_0(1 - u_a^*) + (1 - k_0)(-1 - u_c^*). \end{aligned} \quad (29)$$

With the help of (19), it is easy to find an equivalent zero-sequence signal for an arbitrary distribution of zero vectors, and the opposite is true. Here are some typical examples.

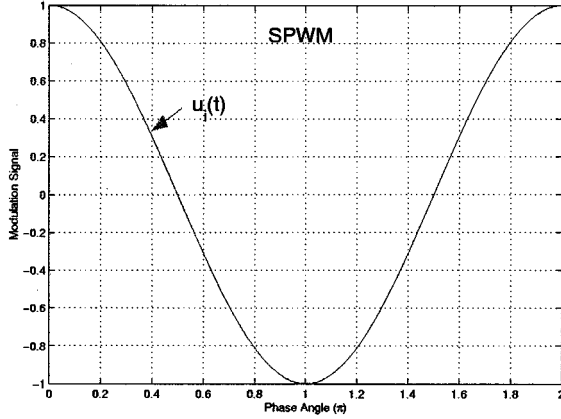
1) *Continuous PWM*: $c_i(t) = 0$ yields sinusoidal carrier-based PWM with maximum modulation index $m_{\text{max}} = 1$ in the linear modulation range as shown in Fig. 7(a). According to (19), its equivalent distribution of T_0 and T_7 in sector I is

$$\begin{aligned} T_0 &= \frac{T_s}{2} (1 - m \cos(\varphi)) \\ T_7 &= T_s - T_1 - T_2 - T_0. \end{aligned} \quad (30)$$

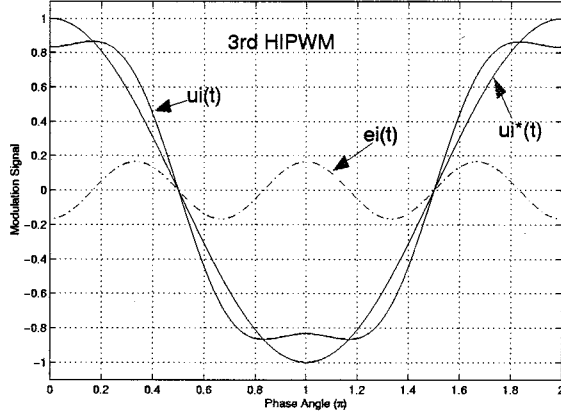
$c_i(t) = m/6 \sin(3\varphi)$ leads to third harmonics injection PWM (HIPWM) [2] with maximum modulation index

TABLE IV
SPACE-VECTOR SECTORS AND FUNDAMENTAL MODULATION SIGNALS

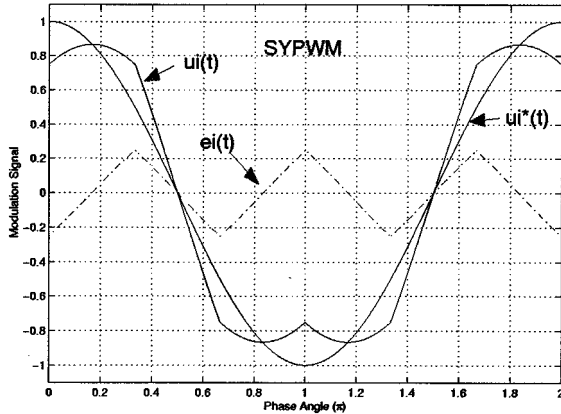
Sector I	Sector II	Sector III	Sector IV	Sector V	Sector VI
$u_a^* > u_b^* > u_c^*$	$u_b^* > u_a^* > u_c^*$	$u_b^* > u_c^* > u_a^*$	$u_c^* > u_b^* > u_a^*$	$u_c^* > u_a^* > u_b^*$	$u_a^* > u_c^* > u_b^*$



(a)



(b)

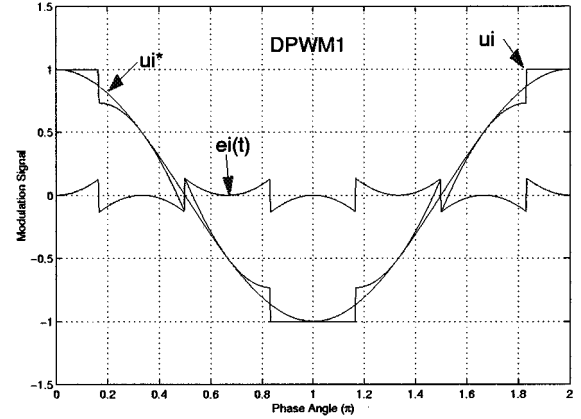


(c)

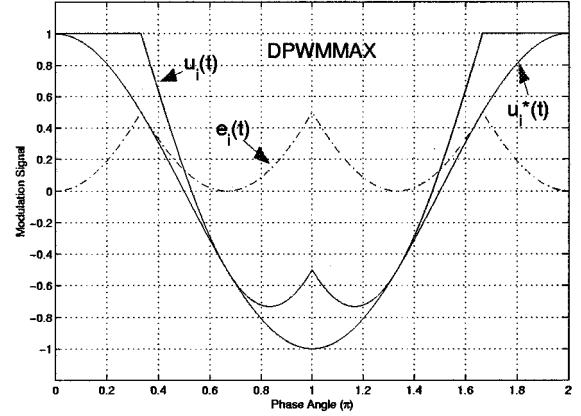
Fig. 7. Modulation signals of continuous PWM ($m = 1.0$). (a) SPWM. (b) HIPWM. (c) SYPWM.

$m_{\max} = 2/\sqrt{3}$ in the linear modulation range as shown in Fig. 7(b). Its corresponding T_0 and T_7 in sector I are

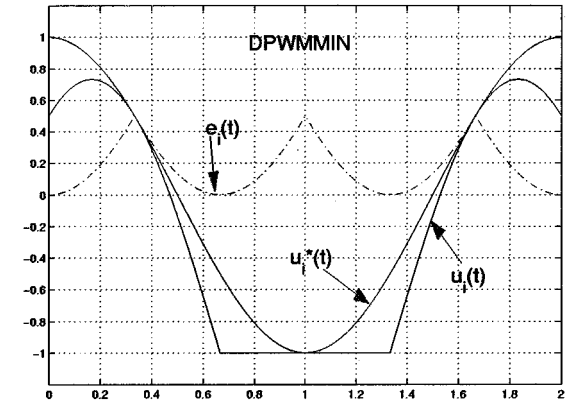
$$\begin{aligned} T_0 &= \frac{T_s}{2} \left[1 - m(\cos(\varphi) - \frac{1}{6} \cos(3\varphi)) \right] \\ T_7 &= T_s - T_1 - T_2 - T_0. \end{aligned} \quad (31)$$



(a)



(b)



(c)

Fig. 8. Modulation signals of discontinuous PWM ($m = 1.0$). (a) DPWM1. (b) DPWMMAX. (c) DPWMMIN.

$e_i(t) = 1/2(1 - u_{\max}^*) + 1/2(-1 - u_{\min}^*)$ brings symmetrical PWM (SYPWM) [18], [20] with maximum modulation index $m_{\max} = 2/\sqrt{3}$ in the linear modulation range as shown in Fig. 7(c). Its corresponding T_0 and T_7 in sector I are

$$T_0 = T_7 = \frac{1}{2}(T_s - T_1 - T_2). \quad (32)$$

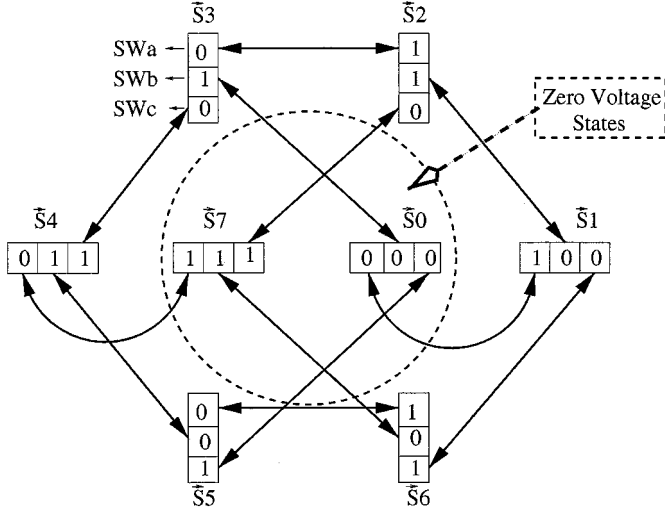


Fig. 9. Transitions between different switching states.

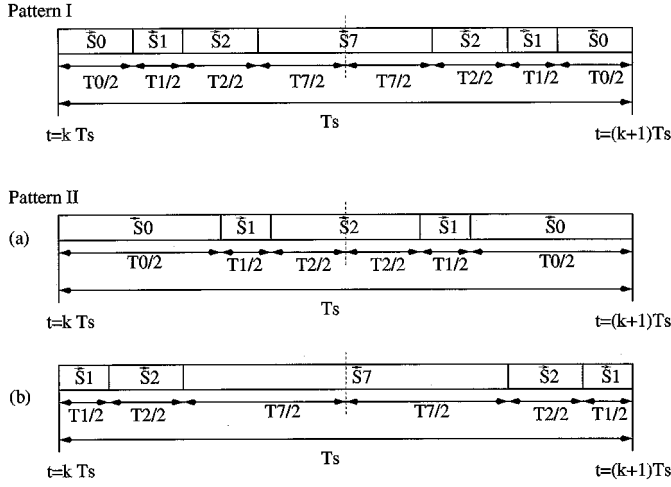


Fig. 10. Equivalent switching patterns for double-edge carrier-based PWM.

2) *Discontinuous PWM (DPWM)*: For DPWM1 [24] as shown in Fig. 8(a), $e_i(t)$ can be expressed by

$$e_i = \begin{cases} 1 - u_{\max}^* & |u_{\max}^*| \geq |u_{\min}^*| \\ -1 - u_{\min}^* & |u_{\max}^*| < |u_{\min}^*| \end{cases} \quad (33)$$

DPWM1's equivalent distribution of T_0 and T_7 [14] in sector I are

$$\begin{aligned} T_0 &= T_s - T_1 - T_2 \quad (0 \leq \varphi < \frac{\pi}{6}; T_7 = 0) \\ T_7 &= T_s - T_1 - T_2 \quad (\frac{\pi}{6} \leq \varphi < \frac{\pi}{3}; T_0 = 0). \end{aligned} \quad (34)$$

For DPWM with $e_i(t) = 1 - u_{\max}^*$ (DPWMMAX) its equivalent distribution of zero vectors is $T_0 = 0$ and $T_7 = T_s - T_1 - T_2$ in all six space-vector sectors [as shown in Fig. 8(b)].

For DPWM with $e_i(t) = -1 - u_{\min}^*$ (DPWMMIN), its equivalent distribution of zero vectors is $T_7 = 0$ and $T_0 = T_s - T_1 - T_2$ in all six space-vector sectors [as shown in Fig. 8(c)].

The leading feature of DPWM is that the switching actions of a DPWM modulator are $2/3$ as much as those of a continuous PWM modulator with identical carrier frequency. Fewer switching actions leads to less switching loss. The maximum modulation index m_{\max} for all DPWM modulators is $2/\sqrt{3}$ in the linear modulation range.

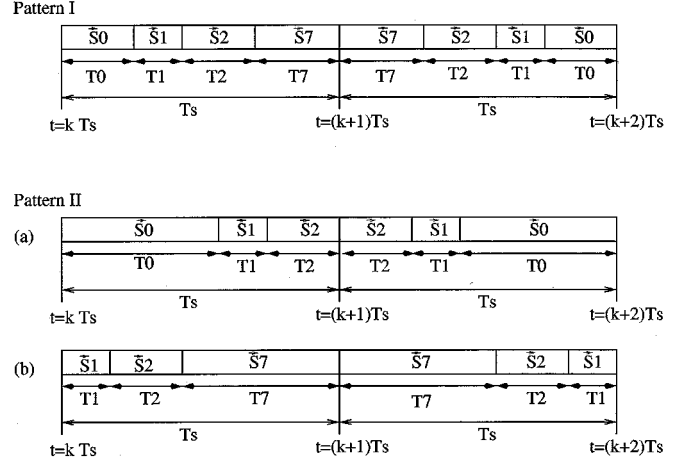


Fig. 11. Equivalent switching patterns for single-edge carrier-based PWM.

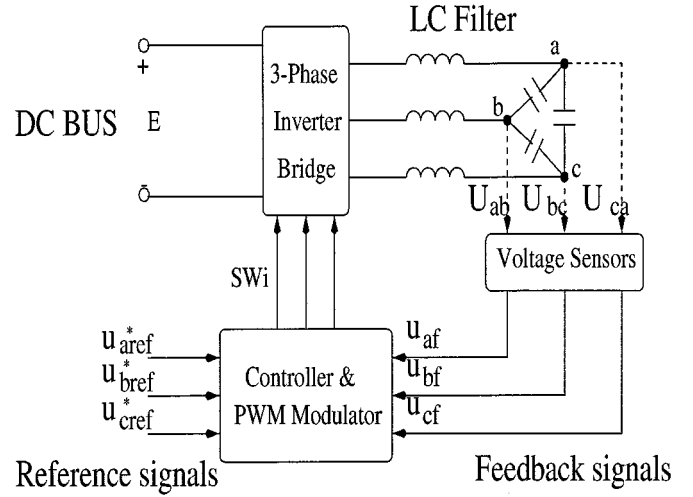


Fig. 12. Instantaneous feedback CVCF PWM inverter.

E. Switching Pattern of Space-Vector Modulation and Carrier Type

When the modulation signals with frequency f and a carrier with frequency f_{car} are determined, a carrier-based PWM modulator is determined. The main performance of a carrier-based PWM modulator is determined by its modulation signals. However, a carrier affects the superior performance of the modulator, too.

The main function of the space-vector modulation strategy is to determine the pulsewidth for active vectors within each sampling interval (i.e., voltage-second average over that interval) which contributes fundamental components in the line-to-line voltages. The optimal sequence of the pulse within the sampling interval leads to a superior-performing space-vector modulation modulator. In this section, the relationship between carrier type and switching pattern of space-vector modulation is discussed.

Fig. 9 shows all the possible transitions between different switching states, every single arrow representing one switching action only. For example, a transition from state S_0 to S_1 needs switching action of at least one bridge leg, while the transition from S_1 to S_4 needs at least three switching actions [3], [17]. It shows that the switching pattern of the space-vector modulation

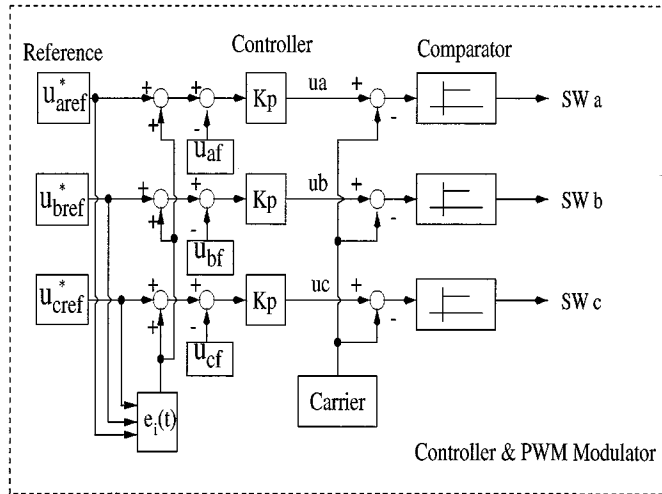


Fig. 13. Conventional nonsinusoidal PWM modulator implementation.

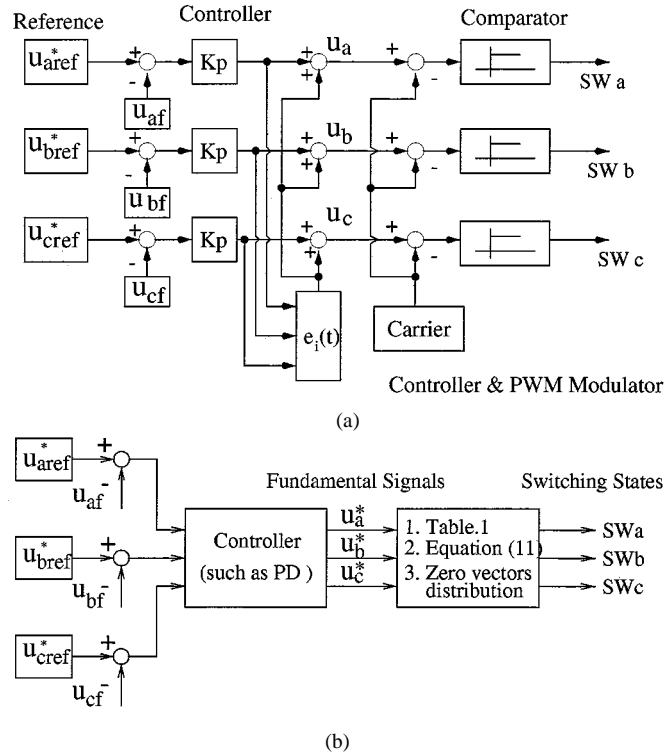
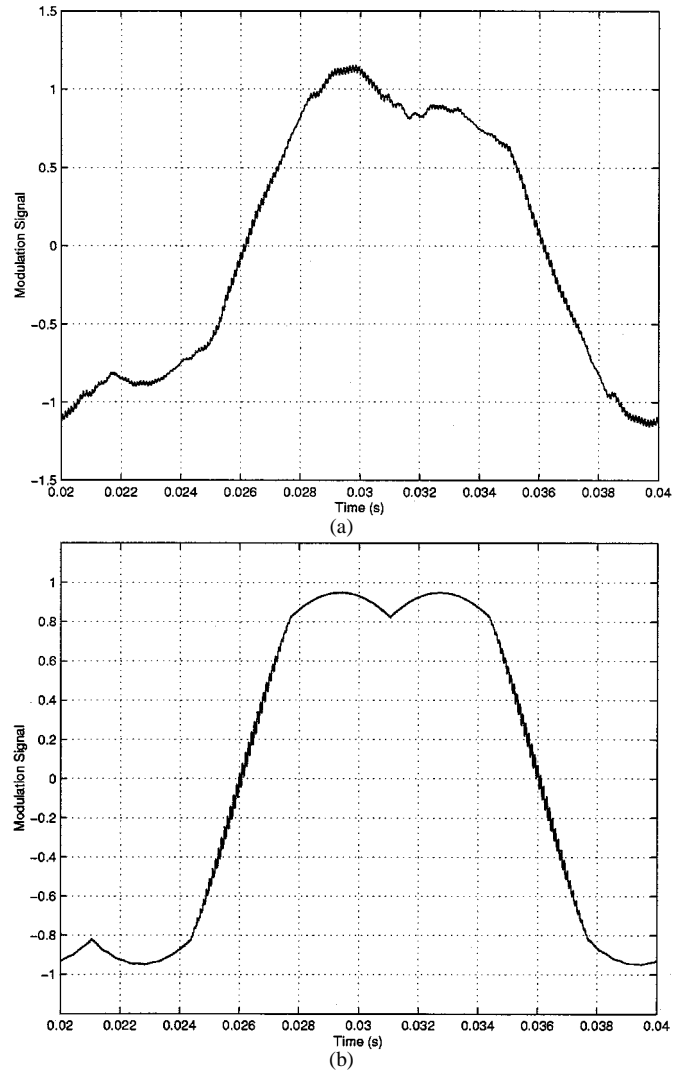


Fig. 14. Closed-loop feedback PWM modulator implementation. (a) Nonsinusoidal carrier-based PWM modulator. (b) Space-vector PWM modulator.

in one sampling interval does affect the number of switching actions. Fewer switching actions leads to less switching loss. All transitions between arbitrary two successive space vectors for the optimal switching pattern need only one switching action (as shown in Fig. 9).

In Figs. 10 and 11, two kinds of optimal switching pattern of space vectors in sector I are displayed. Pattern I which adopts both S_0 and S_7 in one sampling interval is corresponding to continuous PWM. Pattern II which uses only one zero switching state, either S_0 or S_7 , is corresponding to discontinuous PWM.

Fig. 10 shows the equivalent switching pattern of space-vector modulation for the center-pulse double-edge carrier-based

Fig. 15. Simulation results of two implementation methods ($m = 1.0$). (a) Conventional SYPWM. (b) Feedback SYPWM.

PWM with a carrier frequency $1/T_s$. The typical carrier for the double-edge carrier-based PWM is the triangle carrier. In pattern I, there are six switching actions for the three legs of the inverter during one sampling interval. In pattern II, there are four switching actions in one sampling interval. The number of switching actions for pattern II is only 67% of that of pattern I.

Fig. 11 shows the equivalent switching patterns for the back-to-back single-edge carrier-based PWM with a carrier frequency $1/T_s$. The typical carrier for the single-edge carrier-based PWM is the sawtooth carrier. In pattern I, there are three switching actions for the three legs of the inverter during one sampling interval. In pattern II, there are two switching actions in one sample action. The overall switching frequency of pattern II is only 67% of that of pattern I. It shows that, at the same sampling frequency $1/T_s$, the switching actions of pattern I (or II) in Fig. 11 is 1/2 as much as that of corresponding pattern I (or II) in Fig. 10.

Furthermore, the center-pulse switching pattern results in minimization of the harmonic distortion of the inverter currents [5], [26].

V. CLOSED-LOOP FEEDBACK PWM MODULATOR

All the modulators discussed open-loop PWM modulators. In a closed-loop feedback PWM system as shown in Fig. 12, the fundamental components $u_i(t)$ of modulation signals $u_i(t)$ are generated by the sum of reference signals $u_{a\text{ref}}^*(t), u_{b\text{ref}}^*(t), u_{c\text{ref}}^*(t)$ and feedback voltages $u_{af}(t), u_{bf}(t), u_{cf}(t)$. Fig. 12 shows a closed-loop feedback constant-voltage constant-frequency (CVCF) PWM inverter. In this inverter, nonsinusoidal PWM modulators, such as HIPWM, SYPWM, etc., cannot be implemented as shown in Fig. 13, otherwise m_{max} of the linear modulation range $\leq 2/\sqrt{3}$. The carrier-based PWM modulators should be implemented as shown in Fig. 14(a). Its corresponding space-vector modulation modulator should be implemented as shown in Fig. 14(b). In Fig. 14(b), Table III is used to locate the space vector sector, and Table IV is used to compute corresponding active space vectors. Therefore, the appropriate modulation signals or space vectors can be generated.

Fig. 15 shows the simulation results of the conventional implementation and feedback implementation of an SYPWM modulator. Fig. 15(a) shows that overmodulation occurs (i.e., modulation signal > 1) with modulation index $m = 1.0$ and the modulation signal is distorted; Fig. 15(b) shows modulation is inside the linear range with $m = 1.0$ and the modulation signal waveform is the same as the modulation signal as shown in Fig. 7(c).

From a practical viewpoint, it is more important to study the closed-loop feedback PWM. The essence of the problem is how to generate the zero-sequence signal or zero vectors properly. It should be highlighted that the maximum index m_{max} in the linear modulation range for closed-loop feedback PWM is $2/\sqrt{3}$ with a suitable zero-sequence signal or zero vectors.

VI. CONCLUSIONS

In this paper, the relationship between the carrier-based PWM and space-vector modulation was comprehensively investigated. The relationships between the modulation signals (include fundamental signals and zero-sequence signal) and space vectors, between the modulation signals and space-vector sectors, and between the switching pattern of space-vector modulation and the type of carrier were discussed and established. All the relationships provide a universal platform not only to implement transformation between carrier-based PWM and space-vector modulation, but also to develop different performance PWM modulators. All the analyses are independent of the load type. It indicates that the possible maximum modulation index m_{max} for all PWM modulators is $2/\sqrt{3}$ in the linear modulation range. Furthermore, the problem of feedback PWM was highlighted with corresponding solutions. Simulation results were provided to support the claims.

REFERENCES

- [1] S. R. Bowes, "New sinusoidal pulsewidth modulated inverter," *Proc. Inst. Elect. Eng.*, vol. 122, pp. 1279–1285, 1975.
- [2] J. A. Houldsworth and D. A. Grant, "The use of harmonic distortion to increase the output voltage of a three-phase PWM inverter," *IEEE Trans. Ind. Applicat.*, vol. 20, pp. 1224–1228, Sept./Oct. 1984.
- [3] J. Holtz, "Pulsewidth modulation for electronic power conversion," *Proc. IEEE*, vol. 82, pp. 1194–1214, Aug. 1994.
- [4] V. G. Agelidis, P. D. Ziogas, and G. Joos, "'Dead-band' PWM switching patterns," *IEEE Trans. Power Electron.*, vol. 11, pp. 523–531, July 1996.
- [5] A. Trzynadlowski and S. Legowski, "Minimum-loss vector PWM strategy for three-phase inverter," *IEEE Trans. Power Electron.*, vol. 9, pp. 26–34, Jan. 1994.
- [6] M. A. Boost and P. D. Ziogas, "State-of-the-art carrier PWM techniques: A critical evaluation," *IEEE Trans. Ind. Applicat.*, vol. 24, pp. 271–280, Mar./Apr. 1988.
- [7] P. D. Ziogas, L. Moran, G. Joos, and D. Vincenti, "A refined PWM scheme for voltage and current source converter," in *Proc. IEEE PESC'90*, 1990, pp. 977–983.
- [8] H. W. v. d. Brocker, H. C. Skudenly, and G. Stanke, "Analysis and realization of a pulse width modulator based on the voltage space vectors," in *Conf. Rec. IEEE-IAS Annu. Meeting*, Denver, CO, 1986, pp. 244–251.
- [9] O. Ogasawara, H. Akagi, and A. Nabel, "A novel PWM scheme of voltage source inverters based on space vector theory," in *Proc. EPE European Conf. Power Electronics and Applications*, 1989, pp. 1197–1202.
- [10] M. Depenbrock, "Pulsewidth control of a 3-phase inverter with nonsinusoidal phase voltages," in *Proc. IEEE-IAS Int. Semiconductor Power Conversion Conf.*, Orlando, FL, 1975, pp. 389–398.
- [11] J. Holtz, "Pulsewidth modulation — A survey," in *Proc. IEEE PESC'92*, 1992, pp. 11–18.
- [12] J. Holtz, W. Lotzkat, and A. Khambadkone, "On continuous control of PWM inverters in the overmodulation range including the six-step mode," in *Proc. IEEE IECON'92*, 1992, pp. 307–312.
- [13] B. K. Bose and H. A. Sutherland, "A high performance pulsewidth modulator for an inverter-fed drive system using a microcomputer," *IEEE Trans. Ind. Applicat.*, vol. 19, pp. 235–243, Mar./Apr. 1983.
- [14] A. M. Hava, R. Kerkman, and T. A. Lipo, "Carrier-based PWM-VSI overmodulation strategies: Analysis, comparison, and design," *IEEE Trans. Power Electron.*, vol. 13, pp. 674–689, July 1998.
- [15] D. W. Chung, J. S. Kim, and S. K. Sul, "Unified voltage modulation technique for real-time three-phase power conversion," *IEEE Trans. Ind. Applicat.*, vol. 34, pp. 374–380, Mar./Apr. 1998.
- [16] J. W. Kolar, H. Ertl, and F. C. Zach, "Minimizing the current harmonics rms value of three-phase PWM converter system by optimal and suboptimal transition between continuous and discontinuous modulation," in *Proc. IEEE PESC'91*, June 1991, pp. 372–381.
- [17] D. Jenni and F. Wueest, "The optimization parameters of space vector modulation," in *Proc. 5th European Conf. Power Electronics and Applications*, 1993, pp. 376–381.
- [18] V. Blasko, "Analysis of a hybrid PWM based on modified space-vector and triangle-comparison method," *IEEE Trans. Ind. Applicat.*, vol. 33, pp. 756–764, May/June 1997.
- [19] D. G. Holmes, "The general relationship between regular-sampled pulse-width-modulation and space vector modulation for hard switched converters," in *Conf. Rec. IEEE-IAS Annu. Meeting*, 1992, pp. 1002–1009.
- [20] J. W. Kolar, H. Ertl, and F. C. Zach, "Influence of the modulation method on the conduction and switching losses of a PWM converter system," in *Conf. Rec. IEEE-IAS Annu. Meeting*, Seattle, WA, Oct 1990, pp. 502–512.
- [21] S. R. Bowes and Y. S. Lai, "The relationship between space-vector modulation and regular-sampled PWM," *IEEE Trans. Power Electron.*, vol. 14, pp. 670–679, Sept. 1997.
- [22] T. M. Rowan, R. J. Kerman, and T. A. Lipo, "Operation of naturally sampled current regulators in transition mode," *IEEE Trans. Ind. Applicat.*, vol. 23, pp. 586–596, July/Aug. 1987.
- [23] V. Kaura and V. Blasko, "A new method to extend linearity of a sinusoidal PWM in the overmodulation region," *IEEE Trans. Ind. Applicat.*, vol. 32, pp. 1115–1121, Sept./Oct. 1996.
- [24] S. R. Bowes, "Discussion of an algebraic algorithm for microcomputer-based (direct) inverter pulsewidth modulation," *IEEE Trans. Ind. Applicat.*, vol. 24, pp. 888–893, Nov./Dec. 1988.
- [25] A. M. Hava, R. Kerkman, and T. A. Lipo, "A high-performance generalized discontinuous PWM algorithm," *IEEE Trans. Ind. Applicat.*, vol. 34, pp. 1059–1071, Sept./Oct. 1998.
- [26] D. G. Holmes, "The significance of zero space vector placement for carrier-based PWM schemes," *IEEE Trans. Ind. Applicat.*, vol. 32, pp. 1122–1129, Sept./Oct. 1996.



Kelian Zhou was born in Hubei, China, in 1970. He received the B.S. degree from Huazhong University of Science and Technology, Wuhan, China, and the M.E.E degree from Wuhan University of Transportation, Wuhan, China, in 1992 and 1995, respectively, both in electrical engineering. He is currently working toward the Ph.D degree at Nanyang Technological University, Singapore.

His research interests are in the fields of power electronics and electric machines, advanced control theory, and applications.



Danwei Wang (S'88–M'89) received the B.E. degree from South China University of Technology, Guangzhou, China, and the M.S.E. and Ph.D. degrees from the University of Michigan, Ann Arbor, in 1982, 1985, and 1989, respectively.

Since 1989, he has been with the School of Electrical and Electronic Engineering, Nanyang Technological University, Singapore, where he is an Associate Professor. His research interests include robotics, control theory, and applications.

He has authored publications in the areas of manipulator/mobile robot dynamics, path planning, robust control, iterative learning control, and adaptive control, and their applications to industrial systems.